Unique Performance and Characterization of a Crystalline $SbRe_2O_6$ Catalyst for Selective Ammoxidation of Isobutane

Haichao Liu and Yasuhiro Iwasawa*

Department of Chemistry, Graduate School of Science, The University of Tokyo, Hongo, Bunkyo-ku, Tokyo 113-0033, Japan

Received: October 8, 2001; In Final Form: December 10, 2001

The catalytic performances of a new family of crystalline Re−Sb−O compounds $SbRe_2O_6$, $SbOReO_4{\cdot}2H_2O$ and $Sb_4Re_2O_{13}$ in selective ammoxidation of isobutane (i-C_4H_{10}) to methacrylonitrile (MAN) have been studied and compared with those of a mechanical mixture of $Sb_2O_3 + Re_2O_7$, coprecipitated $SbRe_2O_x$, Sb_2O_3-supported Re_2O_7, bulk Re oxides, and Sb oxides. $SbRe_2O_6$ efficiently catalyzed the i-C_4H_{10} ammoxidation to MAN at 673 K with the good selectivity to MAN (44.9%) and to the sum of MAN + i-C_4H_8 (84.3%) at a steady-state conversion of 4.4%, while significantly no MAN activity was observed on the other catalysts. No structural change in the bulk and surface of $SbRe_2O_6$ after the i-C_4H_{10} ammoxidation was observed by means of X-ray diffraction (XRD), X-ray photoelectron spectroscopy (XPS), scanning electron microscopy (SEM), and in situ confocal laser Raman microscopic spectroscopy (LRM). The good performance of $SbRe_2O_6$ may be ascribed to its specific crystal structure composed of alternate octahedral $(Re_2O_6)^{3-}$ and $(SbO)^+$ layers. It was found that the presence of NH_3 was prerequisite to the C−H bond breaking of i-C_4H_{10}, and the oxidation/dehydrogenation of i-C_4H_{10} never proceeded in the absence of NH_3. The presence of NH_3 was also prerequisite to maintain the crystal structure of $SbRe_2O_6$ under the reaction conditions. Fourier transformed infrared (FT-IR) spectra showed that NH_x species irreversibly adsorbed on the $SbRe_2O_6$ catalyst. The i-C_4H_{10} ammoxidation proceeded on $SbRe_2O_6$ by a redox mechanism, in which the oxidative dehydrogenation of i-C_4H_{10} to i-C_4H_8 was the rate-determining step. Increasing reaction temperature and decreasing GHSV did not give rise to increase in the formation of byproducts CO_2 and acetonitrile. Thus the crystalline $SbRe_2O_6$ compound may be regarded to be a new promising catalyst for the ammoxidation of light alkanes.

1. Introduction

There is increasing economic incentive in petroleum and chemical industries to directly utilize cheap and abundantly available alkanes as feedstocks in stead of the corresponding alkenes in selective oxidation/ammoxidation reactions to produce unsaturated aldehydes and nitriles. A large number of mixed-oxide catalysts for these reactions have been investigated to date.[1−14] However, owing to the inertness of alkanes, very few catalysts have displayed good performances comparable to those for the corresponding alkene processes, despite the extensive scientific studies. The only commercial example of use of alkane so far is *n*-butane oxidation to maleic anhydride on V−P−O catalysts. Recently, propane ammoxidation to acrylonitrile on Sb−V−O and $MoVNbTeO_x$ catalysts has been examined at the exploratory and pilot plant stages, which could lead to industrially promising selective ammoxidation processes.[4,10,12,14] While these results point out the possibility of selective oxyfunctionalization of light alkanes on oxide catalysts, they allow to acknowledge that the controlled oxyfunctionalization of light alkanes is still one of the major challenges in heterogeneous catalysis. It is thus clearly needed to develop new catalytic materials that are efficient for the selective oxidation/ammoxidation of light alkanes.

To achieve this goal, we have been exploring a new family of mixed Re−Sb oxides as selective oxidation catalysts. Our such choice is based on the following facts and considerations. Re oxides possess redox properties similar to those of V, Mo, and W oxides,[15] which have been extensively used as main components in various oxidation catalysts.[1−4,8−20] So Re may also be a key catalytic element capable of activating hydrocarbons for selective oxidation, notwithstanding the fact that it has found hitherto few applications to the oxidation of methanol and ethanol.[17−24] On the other hand, Sb is well-known to constitute a promoter element in various mixed-oxide formulations such as V−Sb−O, Sn−Sb−O, Mo−Sb−O, Fe−Sb−O, and U−Sb−O.[1−12,25−30] In these catalysts, Sb oxides are considered to facilitate the abstraction of an allylic hydrogen from hydrocarbon molecules as well as the subsequent oxygen or nitrogen insertion into allylic intermediate species. Our recent results concerning the Pt/SbO_x catalyst for the selective oxidation of isobutane and isobutylene to methacrolein also show that the Sb_6O_{13} suboxide phase formed under the catalytic oxidation conditions contributes to the oxygen insertion to allylic intermediates in a synergetic manner with Pt particles.[6−8] Therefore, mixed oxides associated with Re and Sb may be a combination of good choice for development of a new family of catalytic materials for selective ammoxidation of alkanes.

We first employed three crystalline Re−Sb mixed oxides, $SbRe_2O_6$, $SbOReO_4{\cdot}2H_2O$, and $Sb_4Re_2O_{13}$, with different crystal structures as new catalysts for the selective oxidation of i-C_4H_8 and i-C_4H_{10} to methacrolein (MAL).[5,31,32] These mixed oxides are the only three crystalline Re−Sb−O compounds known so far.[24,33,34] It was found that they exhibited promising performances; for example, i-C_4H_{10} was converted to MAL and i-C_4H_8

* To whom correspondence should be addressed. Fax: 81-3-5800-6892. E-mail: iwasawa@chem.s.u-tokyo.ac.jp

10.1021/jp013729i CCC: $22.00
Published on Web 02/09/2002

in a high selectivity of 83% on $SbRe_2O_6$ at 773 K. But a problem encountered under the catalytic oxidation conditions was a partial decomposition of the catalysts, resulting in sublimation and loss of Re oxides. In an effort to overcome the decomposition problem, recently, we have found that *i*-C_4H_{10} ammoxidation to methacrylonitrile (MAN) (eq 1)

$$\text{i-}C_4H_{10} + NH_3 + 2O_2 \rightarrow \text{MAN} + 4H_2O \qquad (1)$$

efficiently proceeded on the $SbRe_2O_6$ catalyst at 673 K with good selectivities to MAN (44.9%) and to the sum of MAN and *i*-C_4H_8 (84.3%), in which no structural change in the $SbRe_2O_6$ crystal occurred.[35,36] The presence of NH_3 in the catalytic system played a double role in not only stabilizing the $SbRe_2O_6$ crystal but also promoting the activity for dehydrogenation of *i*-C_4H_{10}. In this paper, we report a systematic study on the selective *i*-C_4H_{10} ammoxidation catalysis of the three crystalline Re−Sb−O compounds and their characterization by means of X-ray diffraction (XRD), X-ray photoelectron spectroscopy (XPS), scanning electron microscope (SEM), in-situ confocal laser Raman microscopic spectroscopy (LRM), and Fourier transformed infrared spectroscopy (FT-IR). The study aimed at shedding light on the correlation between the catalytic performances of the Re−Sb−O samples and their structural characteristics, as well as the promoting effect of NH_3 on the selective ammoxidation catalysis.

2. Experimental Section

2.1. Preparation of Catalysts. Three crystalline Re−Sb−O compounds $SbOReO_4{\cdot}2H_2O$, $SbRe_2O_6$, and $Sb_4Re_2O_{13}$ were synthesized in procedures similar to those reported previously.[5,24,31−34] Briefly, $SbOReO_4{\cdot}2H_2O$ was synthesized hydrothermally as follows: 2.8 g of Re_2O_7 (Soekawa Chemicals, purity > 99.99%) was dissolved in deionized water (2 mL) in a Teflon-lined autoclave. To the resultant perrhenic acid solution, 1.7 g of Sb_2O_3 (Soekawa Chemicals, purity > 99.99%) was added under vigorous stirring (Sb/Re atomic ratio = 1:1). Afterward, the autoclave was sealed and maintained at 423 K for 24 h, and then at room temperature for 6 days. By drying the resultant compound under vacuum at 343 K, $SbOReO_4{\cdot}2H_2O$ was obtained as white powder. $SbRe_2O_6$ was synthesized through a solid-state reaction between $SbOReO_4{\cdot}2H_2O$ and metallic Re (Soekawa Chemicals, purity > 99.99%) in a 9:5 molar ratio. After the mixture was heated at 773 K for 3 days in a sealed silica tube, the black powder as a main product was formed in the center of the tube, while a small amount of white crystals was formed at its apexes. Then the two compounds were carefully collected separately. The black powder was identified to be $SbRe_2O_6$ by XRD and X-ray fluorescence (XRF). The white crystals were Sb_2O_3, which was formed from the excess of Sb in the mixture of precursors. The synthesis of $Sb_4Re_2O_{13}$ was conducted in a similar way to the case of $SbRe_2O_6$. A mixture of $SbOReO_4{\cdot}2H_2O$ and Sb_2O_3 in a 2:1 molar ratio was heated at 773 K for 6 days in an evacuated silica tube to yield gray crystals of $Sb_4Re_2O_{13}$. The BET surface areas of the three Re−Sb−O compounds were approximately 1 $m^2\ g^{-1}$.

For comparison, a mechanical mixture of Re_2O_7 and Sb_2O_3 (denoted hereinafter as mix.$Re_2O_7{\cdot}Sb_2O_3$) was prepared by gently grinding 0.3 g of Re_2O_7 and 0.3 g of Sb_2O_3 in an agate mortar in a N_2-filled glovebox (as Re_2O_7 is highly hygroscopic). An Sb_2O_3-supported Re_2O_7 catalyst (denoted as Re_2O_7/Sb_2O_3) (Re loading: 10 wt %) was prepared by an impregnation method using an aqueous solution of NH_4ReO_4 (Soekawa Chemicals, purity > 99.9%). A coprecipitated $SbRe_2O_x$ catalyst (denoted as copr.$SbRe_2O_x$) was also prepared by a coprecipitation method using an ethanol solution of $ReCl_3$ and $SbCl_3$, followed by washing with water to eliminate the residual Cl from the catalyst.

2.2. Catalytic Performances. Catalytic ammoxidation reactions were carried out at atmospheric pressure in a continuous-flow fixed-bed glass reactor (6 mm in diameter). The typical composition of reaction feed was 10% *i*-C_4H_{10}, 15% NH_3, and 25% O_2 balanced with He (mol %). The catalytic performance was conducted typically with 0.3 g of catalyst diluted with 1 g of quartz sand to avoid temperature gradients and hot spots in the reactor. Prior to each run, the catalyst was pretreated in a He flow (40 mL min^{-1}) at 673 K for 1 h. Then the reaction feed was introduced into the reactor at a gas-hourly space-velocity (GHSV) of 5000 h^{-1} using digital mass-flow controllers. The reactants and products were analyzed using two on-line gas chromatographs equipped with three columns of Unibeads C at 423 K for O_2, CO, and CO_2, Gaskuropack 54 at 423 K for methacrylonitrile and other oxygenates, and VZ-10 at 348 K for *i*-C_4H_{10}, *i*-C_4H_8 and other hydrocarbons. The steady-state kinetic data were collected after 2 h of time-on-stream. Conversions and selectivities were calculated based on the analysis of the reactants and products detected in the reactor effluent. The total amounts were referred to the reactant feed amount. The carbon balance was always found to be better than 98.5%. The conversion of NH_3 to N_2 (main) and NO_x (trace) was <15% (typically ~10%) under the present reaction conditions.

A blank test of *i*-C_4H_{10} ammoxidation at 673 K was conducted in an empty reactor as well, and no *i*-C_4H_{10} conversion was observed in the homogeneous gas phase under the experimental conditions studied.

2.3. Pulse Reactions. Pulse reactions on the $SbRe_2O_6$ catalyst were carried out at 673 K in an apparatus where pulse and continuous flow reactions can be alternately operated at atmospheric pressure, and He was used as carrier gas at a flow rate of 30 mL min^{-1}. After the $SbRe_2O_6$ catalyst (0.45 g) was pretreated at 673 K under He for 1 h, reaction feed was pulsed into the reactor via a six-port gas sampling valve. The volume of each pulse was approximately 1 mL. The products were analyzed using an on-line GC mentioned above.

2.4. FT-IR Measurement for NH_3 Adsorption. FT-IR spectra were recorded on a JASCO FT/IR-230 spectrometer equipped with a MCT detector with a resolution of 4 cm^{-1}. $SbRe_2O_6$ powder was pressed into self-supported thin wafers and placed in a quartz cell with NaCl windows, which was combined with a closed circulating system. To examine the adsorption of NH_3 on the $SbRe_2O_6$ catalyst, the sample was first heated to 673 K at a ramp rate of 10 K min^{-1} and then kept at 673 K for 1 h in the quartz IR cell under 26.6 kPa of He, followed by evacuation at 673 K for 1 h. After cooling to room temperature, 3.99 kPa of NH_3 was introduced to the IR cell, followed by evacuation of NH_3 at room temperature, or followed by heating to 673 K under 3.99 kPa of NH_3 and then by evacuation at 673 K. To examine the reactivity of adsorbed NH_3 species, a mixture of *i*-C_4H_{10} (2.66 kPa) and O_2 (0.66 kPa) was introduced to the cell at 673 K after exposure to NH_3 and evacuation at 673 K. All the spectra were obtained as difference spectra by subtracting the background spectrum of the sample from the observed spectra.

2.5. Characterization of Catalysts. XRD patterns were measured in air on a Rigaku Miniflex goniometer using Cu Kα radiation (λ = 1.5418 Å) operated at 30 kV and 15 mA. The 2θ angles were scanned from 5° to 60° at a rate of 2° min^{-1}.

TABLE 1: Isobutane Ammoxidation on Different Re−Sb−O Catalysts and Bulk ReO_x and SbO_x at 673 K[a]

	conversion (%)	reaction rate (μmol g-cat $^{-1}$ h^{-1})	selectivity (%)				
			MAN+*i*-C_4H_8	MAN[b]	*i*-C_4H_8	CH_3CN	CO_2
$SbRe_2O_6$	4.4	785.6	84.3	44.9	39.4	4.7	10.2
$SbRe_2O_6$[c]	0	0					
$SbOReO_4 \cdot 2H_2O$	0	0					
$Sb_4Re_2O_{13}$	0	0					
mix.$Re_2O_7 \cdot Sb_2O_3$	0.5	89.3	trace	0	trace	0	~100
copr.$SbRe_2O_x$	0.4	71.4	20.6	0	20.6	0	79.4
Re_2O_7/Sb_2O_3	0.1	17.8	0	0	0	0	100
Re_2O_7	11.6	2071.3	0	0	0	0	100
ReO_3	2.1	374.9	31.5	7.7	23.8	25.7	42.6
ReO_2	5.6	999.9	31.0	9.1	21.9	32.1	36.4
Sb_2O_3	0	0					
Sb_2O_4	0	0					

[a] *i*-$C_4H_{10}/NH_3/O_2/He$ = 10/15/25/50 (mol %); GHSV = 5000 h^{-1}. [b] MAN: methacrylonitrile. [c] In the absence of NH_3; *i*-$C_4H_{10}/O_2/He$ = 10/25/65 (mol %); GHSV = 5000 h^{-1}.

TABLE 2: Catalytic Performances of $SbRe_2O_6$ Pretreated under Different Gas Mixtures at 673 K[a]

		selectivity (%)				
pretreatment	conversion (%)	MAN+*i*-C_4H_8	MAN [b]	*i*-C_4H_8	CH_3CN	CO_2
He	4.4	84.3	44.9	39.4	4.7	10.6
NH_3/He	4.1	86.7	42.4	44.3	5.1	8.2
i-C_4H_{10}/He	4.2	85.6	42.7	42.9	4.3	10.7
reaction feed	4.6	84.4	44.4	40.0	4.9	10.7
O_2/He	0.4	18.5	0	18.5	0	81.5

[a] *i*-$C_4H_{10}/NH_3/O_2/He$ = 10/15/25/50 (mol %); GHSV = 5000 h^{-1}. [b] MAN: methacrylonitrile.

SEM micrographs were taken on a Hitachi S-4500 microscope equipped with a field emission gun, which was operated at 15 kV and 10 μA. Different places of the samples were measured to obtain common features of SEM images.

XPS spectra were collected on a Rigaku XPS 7000 spectrometer using monochromatic Mg Kα radiation (1253.6 eV) at a source power of 200 W. Chamber pressure during the measurement was about 10^{-7} Pa. The binding energies were referred to the adventitious C 1s peak at 284.6 eV. To minimize exposure of the samples to ambient air, after pretreatment under He or NH_3/He or after the ammoxidation reaction under a mixture of *i*-$C_4H_{10}/NH_3/O_2/He$, the samples were rapidly cooled to room temperature under the gas flow, followed by sealing the reactor. Then, in a N_2-filled glovebox, the samples were pressed into disks and attached to XPS sample holders with thin double-sided tape and transferred to the XPS chamber within 1 min. The overlapping Re $4f_{7/2}$ and Re $4f_{5/2}$ peaks were deconvoluted using Gaussian line shapes. Relative peak areas of the former to the latter were fixed at a ratio of 4/3 and the peak separation was also fixed to be 2.4 eV. Full width at half-maximum height (fwhm) was assumed constant for each of the two peaks of Re $4f_{7/2}$ and Re $4f_{5/2}$ for the same species.

Confocal laser Raman microscopy (LRM) spectra were recorded on a JASCO NRS2100 SA spectrometer equipped with an Ar^+ laser (514.5 nm) and a liquid N_2-cooled CCD detector. The resolution was 5 cm^{-1}, and the laser power was set to 2 mW. Raman shifts for all the samples were measured in the range 1100~185 cm^{-1}. To evaluate the micron-scale homogeneity of the surface, about 30 spectra were measured at different spots of a sample. The samples were analyzed in situ in a way similar to that described previously.[31]

3. Results

3.1. Catalytic Performances of Different Re−Sb−O Catalysts. Table 1 presents conversions, reaction rates, and selectivities of three crystalline compounds, $SbRe_2O_6$, $SbOReO_4 \cdot 2H_2O$, and $Sb_4Re_2O_{13}$, in the *i*-C_4H_{10} ammoxidation at 673 K. The performances of mix.Re_2O_7/Sb_2O_3, copr.$SbRe_2O_x$, Re_2O_7/Sb_2O_3, bulk Re_2O_7, ReO_3, ReO_2, Sb_2O_3, and Sb_2O_4 are also listed for comparison. $SbOReO_4 \cdot 2H_2O$, and $Sb_4Re_2O_{13}$, as well as bulk Sb oxides showed no activity. Bulk Re_2O_7 was active but catalyzed solely the combustion of *i*-C_4H_{10} to CO_2. Bulk ReO_3 and ReO_2 produced methacrylonitrile (MAN), but the selectivities were as low as 7.7−9.1% and the main product was CO_2 for both Re oxides. Re_2O_7/Sb_2O_3 and mix.$Re_2O_7 \cdot Sb_2O_3$ samples showed almost no activity for the *i*-C_4H_{10} ammoxidation either. The compound copr.$SbRe_2O_x$ gave a slight activity (0.4% conversion) in oxidative dehydrogenation of *i*-C_4H_{10} to *i*-C_4H_8 (20.6% selectivity), but no formation of MAN was observed. Isobutane combustion was dominant also with this catalyst. Only the $SbRe_2O_6$ among these samples was active for the selective ammoxidation of *i*-C_4H_{10} to MAN. The selectivities to MAN and to the sum of MAN + *i*-C_4H_8 at the steady-state *i*-C_4H_{10} conversion of 4.4% were 44.9% and 84.3%, respectively. It was also found that in the absence of NH_3 in the reactant feed no reaction including dehydrogenation and combustion occurred, as shown in Table 1, indicating no C−H bond breaking took place in the absence of NH_3.

3.2. Catalytic Properties of $SbRe_2O_6$. In the selective oxidation of *i*-C_4H_8 to methacrolein (MAL), the catalytic property of $SbRe_2O_6$ largely depended on the pretreatment atmospheres.[5,31,32] To investigate the effect of the pretreatment of $SbRe_2O_6$ on the *i*-C_4H_{10} ammoxidation, $SbRe_2O_6$ was pretreated at 673 K for 1 h under the following five different atmospheres, i.e., 100% He, 15% NH_3 in He (mol %), 10% *i*-C_4H_{10} in He, 20% O_2 in He, and a reaction mixture containing 10% *i*-C_4H_{10} + 15% NH_3 + 25% O_2 + 50% He. As shown in Table 2, after the pretreatments with He, *i*-C_4H_{10}/He, NH_3/He and the reaction feed, the *i*-C_4H_{10} conversions and MAN selectivities at the steady-state were nearly the same. However, the pretreatment of $SbRe_2O_6$ with O_2/He led to a drastic decrease in both activity and selectivity; a low activity (0.4% conversion) in the dehydrogenation of *i*-C_4H_{10} to *i*-C_4H_8 (18.5% selectivity) but no activity for the MAN synthesis was observed. Hence,

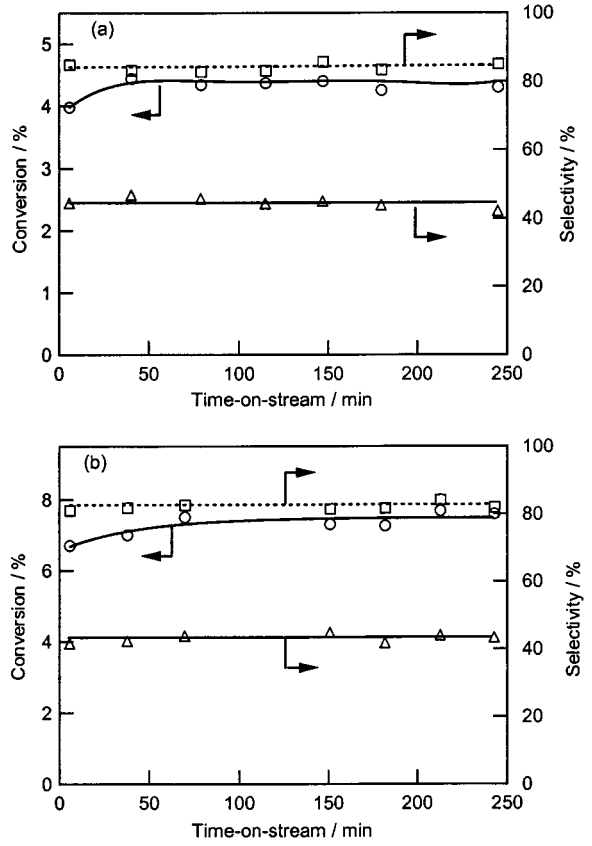

Figure 1. Reaction profiles of the i-C_4H_{10} conversion (○) and the selectivities to the sum of MAN + i-C_4H_8 (□) and to MAN (△) with time-on-stream on $SbRe_2O_6$ at 673 K under GHSV of 5000 h^{-1} (a) and 2500 h^{-1} (b).

the $SbRe_2O_6$ sample subjected to catalytic performance and characterization in this study was pretreated in the He flow.

Figure 1a shows the catalytic behavior of $SbRe_2O_6$ in the i-C_4H_{10} ammoxidation at 673 K as a function of time-on-stream under GHSV of 5000 h^{-1}. It was found that the conversion of i-C_4H_{10} initially increased slightly with time, and then reached a constant value of 4.4%. The selectivities of the MAN and i-C_4H_8 formation (44.9% and 39.4%, respectively) remained almost constant during the test. Decreasing the GHSV from 5000 h^{-1} to 2500 h^{-1} increased the i-C_4H_{10} conversion to 7.5%, while the selectivities to MAN (44.2%) and i-C_4H_8 (38.4%) did not change significantly as shown in Figure 1b.

Figure 2 shows the variation of the conversion and selectivity of the i-C_4H_{10} ammoxidation with reaction temperature in the range 623−773 K. The i-C_4H_{10} conversion increased first with increasing temperature and reached a maximum value at 673 K, then the conversion decreased with further increasing temperature. The selectivity to the sum of MAN + i-C_4H_8 remained almost constant (84.3%) over the whole temperature range, while the MAN selectivity showed an initial increase to reach the constant value as the temperature increased from 623 to 658 K, and inversely, the i-C_4H_8 selectivity decreased from 623 to 658 K before it reached the constant value. The apparent activation energy E_a between 623 and 673 K was estimated to be 213.7 kJ mol^{-1} from the Arrhenius plot for the i-C_4H_{10} conversion. Interestingly, the formation of byproducts acetonitrile and CO_2 was relatively constant between 623 and 773 K. No MAL was formed under these reaction conditions.

The dependencies of reaction rate and selectivity on the partial pressures of i-C_4H_{10}, O_2 and NH_3 at a constant GHSV of 5000 h^{-1} are shown in Figures 3−5, respectively. The rates of the

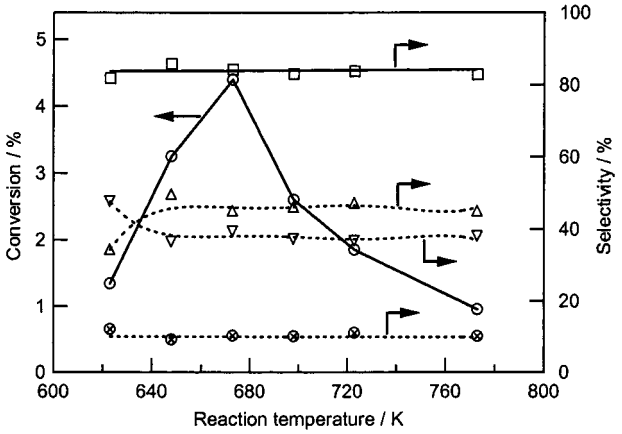

Figure 2. Catalytic performances of $SbRe_2O_6$ in the i-C_4H_{10} ammoxidation as a function of reaction temperature. ○: i-C_4H_{10} conversion; □: selectivity to MAN + i-C_4H_8; △: selectivity to MAN; ▽: selectivity to i-C_4H_8; ⊗: selectivity to CO_2.

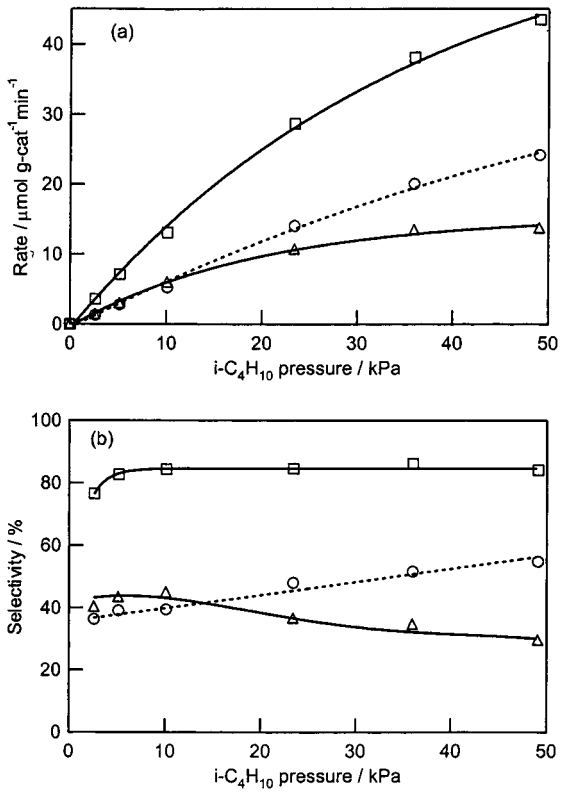

Figure 3. The reaction rates (a) and selectivities (b) in the i-C_4H_{10} ammoxidation on $SbRe_2O_6$ at 673 K as a function of partial pressure of i-C_4H_{10} (15% NH_3, 25% O_2, balanced with He). □: i-C_4H_{10} conversion; △: MAN formation; ○: i-C_4H_8 formation.

i-C_4H_{10} conversion and i-C_4H_8 formation increased monotonically with i-C_4H_{10} pressure, while the rate of MAN formation increased with more upward curvature than others (Figure 3). The selectivity to the sum of MAN + i-C_4H_8 was independent of the i-C_4H_{10} pressure (84.3%) except the point at very low i-C_4H_{10} pressure of 2.6 kPa, while the i-C_4H_8 selectivity linearly increased with increasing i-C_4H_{10} pressure and the MAN selectivity decreased at the i-C_4H_{10} pressures higher than 10 kPa. As shown in Figure 4, the reaction rates of i-C_4H_{10} conversion, and MAN and i-C_4H_8 formations showed similar dependencies to each other on the partial pressure of O_2, namely, they increased first with increasing pressure and then approached to saturation values at high pressures. The selectivity to the sum of MAN + i-C_4H_8 remained almost constant over the whole

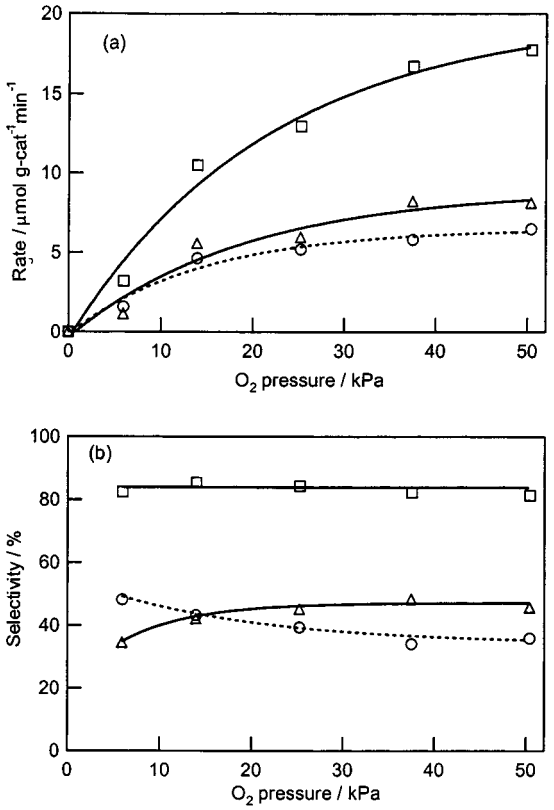

Figure 4. The reaction rates (a) and selectivities (b) in the *i*-C_4H_{10} ammoxidation on $SbRe_2O_6$ at 673 K as a function of partial pressure of O_2 (10% *i*-C_4H_{10}, 15% NH_3, balanced with He). □: *i*-C_4H_{10} conversion; △: MAN formation; ○: *i*-C_4H_8 formation.

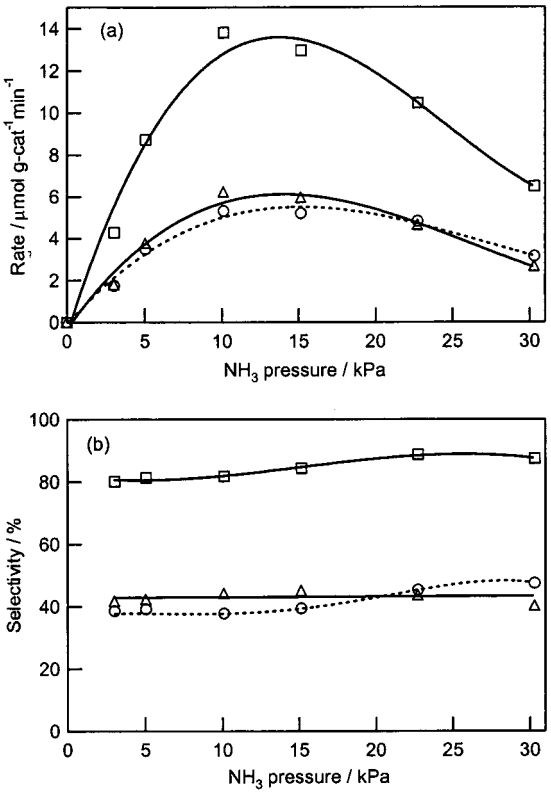

Figure 5. The reaction rates (a) and selectivities (b) in the *i*-C_4H_{10} ammoxidation on $SbRe_2O_6$ at 673 K as a function of partial pressure of NH_3 (10% *i*-C_4H_{10}, 25% O_2, balanced with He). □: *i*-C_4H_{10} conversion; △: MAN formation; ○: *i*-C_4H_8 formation.

pressure range, while the MAN and *i*-C_4H_8 selectivities, respectively, increased and decreased a little with increasing O_2 pressure up to 25 kPa, then showed almost constant values at 25−50 kPa (Figure 4). The feature of Figure 5 is different from those in Figures 3 and 4. At low partial pressures of NH_3, the rates of *i*-C_4H_{10} conversion, and MAN and *i*-C_4H_8 formations increased to maximum values with increasing pressure. After passing through the maximum values around 15 kPa, the rates decreased with further increase of the NH_3 pressure. The selectivities were roughly unchanged with the NH_3 pressure though there were slight changes.

The reaction orders for the *i*-C_4H_{10} conversion, and the MAN and *i*-C_4H_8 formations with respect to the partial pressures of *i*-C_4H_{10}, O_2, and NH_3 at 5−15 kPa were estimated from the data in Figures 3−5, and the reaction rates are given by eqs 2−4.

$$\text{rate } (i\text{-}C_4H_{10} \text{ conversion}) = k(P_{i-C4H10})^{0.91}(P_{O2})^{0.73}(P_{NH3})^{0.75} \quad (2)$$

$$\text{rate (MAN formation)} = k(P_{i-C4H10})^{0.77}(P_{O2})^{0.81}(P_{NH3})^{0.78} \quad (3)$$

$$\text{rate } (i\text{-}C_4H_8 \text{ formation}) = k(P_{i-C4H10})^{1.05}(P_{O2})^{0.62}(P_{NH3})^{0.74} \quad (4)$$

3.3. Pulse Reactions. Five types of pulse experiments were conducted on the $SbRe_2O_6$ catalyst: (i) pulses of a mixture of *i*-C_4H_{10}/NH_3/O_2/He (10/12/18/70, mol %), (ii) pulses of a mixture of *i*-C_4H_{10}/NH_3/He (10/12/78), (iii) pulses of a mixture of *i*-C_4H_{10}/He (10/90) on NH_3-preadsorbed $SbRe_2O_6$, (iv) pulses of a mixture of *i*-C_4H_{10}/O_2/He (10/18/72) on NH_3-preadsorbed $SbRe_2O_6$, and (v) for comparison, pulses of a mixture of *i*-C_4H_{10}/He or *i*-C_4H_{10}/O_2/He on the $SbRe_2O_6$ catalyst without NH_3 pretreatment.

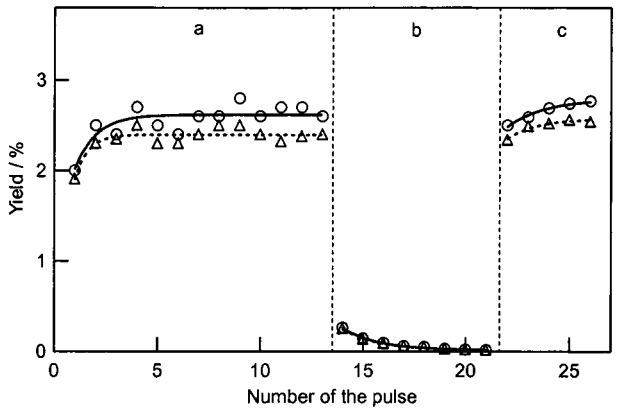

Figure 6. The reaction profile in the pulse experiment on $SbRe_2O_6$ at 673 K; MAN (○) and *i*-C_4H_8 (△) yields as a function of the number of the pulses of *i*-C_4H_{10}/NH_3/O_2/He (= 10/12/18/70, mol %) (a and c), and *i*-C_4H_{10}/NH_3/He (= 10/12/78) (b).

Figure 6 shows that the pulses of a mixture of *i*-C_4H_{10}/NH_3/O_2/He on fresh $SbRe_2O_6$, similar to the steady-state reaction condition, produced MAN and *i*-C_4H_8 selectively with the yields of 2.6% and 2.4%, respectively. Then the pulse was switched to the pulse of the *i*-C_4H_{10}/NH_3/He mixture without O_2. Both MAN and *i*-C_4H_8 yields in the first pulse were only about 10% of the yields for the *i*-C_4H_{10}/NH_3/O_2/He pulse. The MAN and *i*-C_4H_8 formations diminished with further pulses. After the *i*-C_4H_{10} conversion became negligible, the *i*-C_4H_{10}/NH_3/O_2/He mixture was pulsed into the reactor again, resulting in the recovery of the MAN and *i*-C_4H_8 yields as shown in Figure 6.

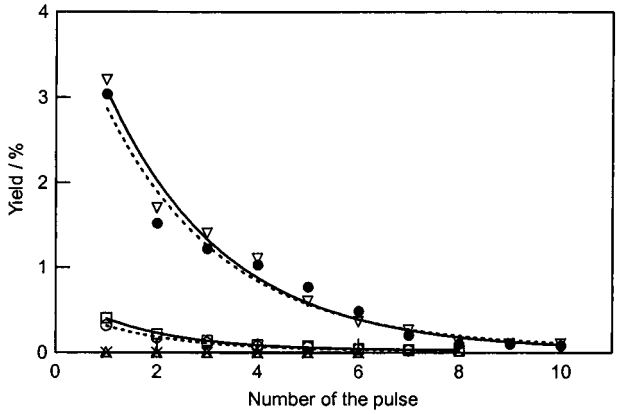

Figure 7. The reaction profiles in the pulse experiments at 673 K; yields of MAN (▽, □) and *i*-C_4H_8 (●, ○) as a function of the numbers of pulses of *i*-C_4H_{10} alone (10% in He, mol %) (□, ○) and a mixture of *i*-C_4H_{10}/O_2/He (10/12/18/70) (▽, ●) on an NH_3-preadsorbed $SbRe_2O_6$ catalyst, and yields of MAL + *i*-C_4H_8 as a function of the numbers of pulses of *i*-C_4H_{10} alone (10% in He) (×) and a mixture of *i*-C_4H_{10}/O_2/He (10/12/18/70) (△) on a $SbRe_2O_6$ catalyst without NH_3 pretreatment.

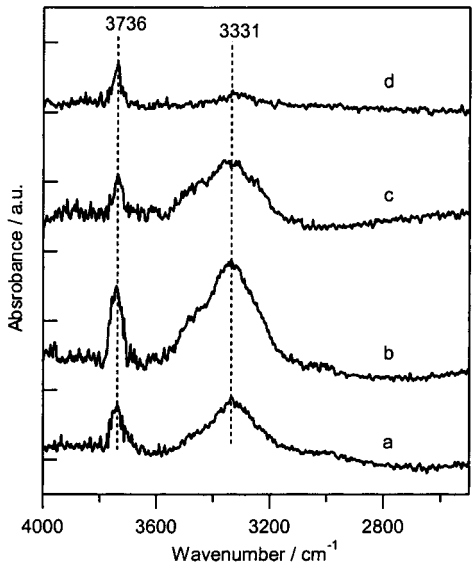

Figure 8. FT-IR spectra for NH_3 adsorbed on $SbRe_2O_6$ (a) after exposure to NH_3 (3.99 kPa) and evacuation at 298 K; (b) after exposure to NH_3 at 673 K, followed by evacuation at 298 K; (c) after exposure to NH_3 at 673 K, followed by evacuation at 673 K; (d) after exposure of (c) to a mixture of *i*-C_4H_{10} (2.66 kPa) + O_2 (0.66 kPa) at 673 K for 5 min.

Variation of the MAN and *i*-C_4H_8 yields with the pulses of a mixture of *i*-C_4H_{10}/O_2/He on NH_3-preadsorbed $SbRe_2O_6$ is shown in Figure 7. A fresh $SbRe_2O_6$ catalyst was pretreated with NH_3 pulses. The NH_3-saturated catalyst was exposed to the *i*-C_4H_{10}/O_2/He pulses. It was found that the first pulse produced MAN and *i*-C_4H_8 in high yields, then the yields decreased with increasing pulses eventually to zero. Upon pulsing *i*-C_4H_{10} alone (in the absence of O_2) on the NH_3-preadsorbed $SbRe_2O_6$ catalyst, MAN and *i*-C_4H_8 were also produced, but their yields were 0.35%, which was 1 order of magnitude lower than the steady-state values. It is to be noted that when the $SbRe_2O_6$ catalyst without NH_3 pretreatment was exposed to pulses of *i*-C_4H_{10}/He and *i*-C_4H_{10}/O_2/He, no *i*-C_4H_{10} conversion occurred at all, as shown in Figure 7, which is consistent with the results in the steady-state flow reaction without NH_3 in Table 1. The treated NH_3 was incorporated into MAN product. In the absence of NH_3 the *i*-C_4H_{10} dehydrogenation to *i*-C_4H_8 never proceeded.

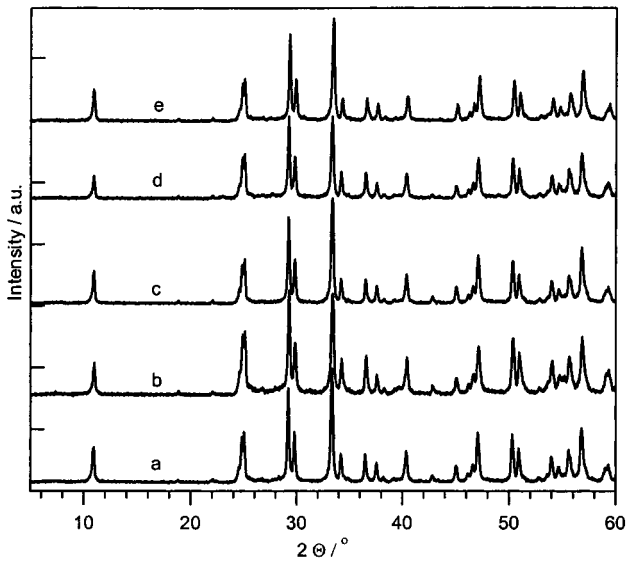

Figure 9. XRD patterns for $SbRe_2O_6$ before (a) and after the pretreatments under (b) He and (c) NH_3/He at 673 K for 1 h, and *i*-C_4H_{10} ammoxidation (d) at 673 K and (e) at 773 K for 3 h.

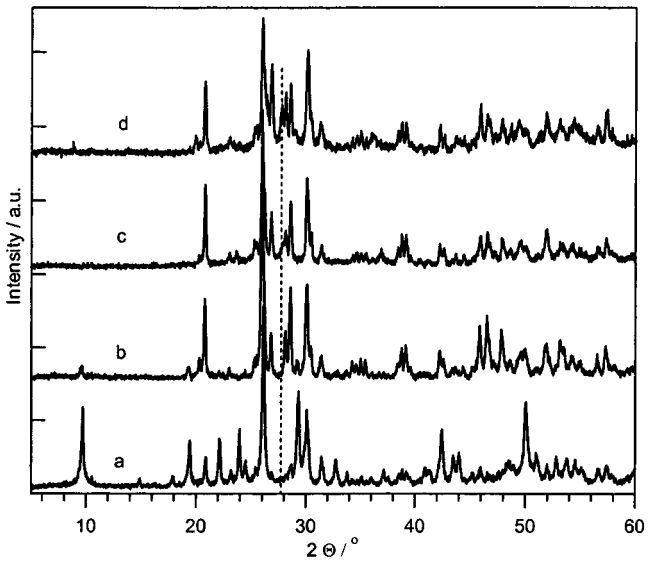

Figure 10. XRD patterns for fresh $SbOReO_4 \cdot 2H_2O$ (a) and $Sb_4Re_2O_{13}$ (b) and $SbOReO_4 \cdot 2H_2O$ (c) and $Sb_4Re_2O_{13}$ (d) after the *i*-C_4H_{10} ammoxidation at 673 K for 3 h. The dashed line shows the XRD peak for Sb_2O_3 phase.

3.4. FT-IR Spectra for NH_3 Adsorption. Figure 8 shows the FT-IR spectra of NH_3 adsorbed on the $SbRe_2O_6$ catalyst. After the admission of NH_3 to the system and evacuation at room temperature, two new peaks at 3331 and 3736 cm^{-1} were observed. After exposure of the fresh catalyst to NH_3 at 673 K for 30 min, followed by evacuation of NH_3 at room temperature, the intensity of the two peaks increased, while there was no significant change in their frequencies. By heating at 673 K in a vacuum, these two peaks still remained, but the peak intensity decreased as shown in Figure 8. Upon NH_3 adsorption at 673 K, followed by exposure to a *i*-C_4H_{10}/O_2 mixture for 5 min at 673 K, the peak at 3331 cm^{-1} almost diminished, while the peak at 3736 cm^{-1} did not change significantly. The peaks at 3736 and 3331 cm^{-1} may be assigned to the stretching vibrations of O−H bond of hydroxyl groups and N−H bond of adsorbed ammonia species, respectively. The bending vibration bands around 1600 cm^{-1} were not detected because of the very low transmittance of the black $SbRe_2O_6$ sample.

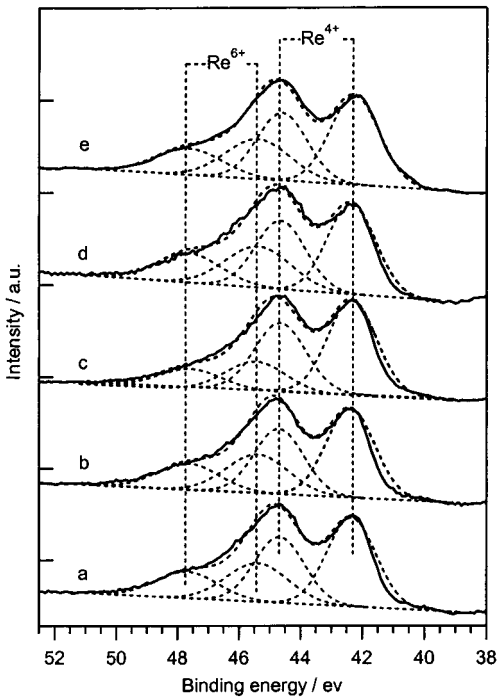

Figure 11. Re 4f XPS spectra for $SbRe_2O_6$ before (a) and after the pretreatments under He (b) and NH_3/He (c) at 673 K for 1 h, and the i-C_4H_{10} ammoxidation at 673 K (d) and 773 K (e) for 3 h.

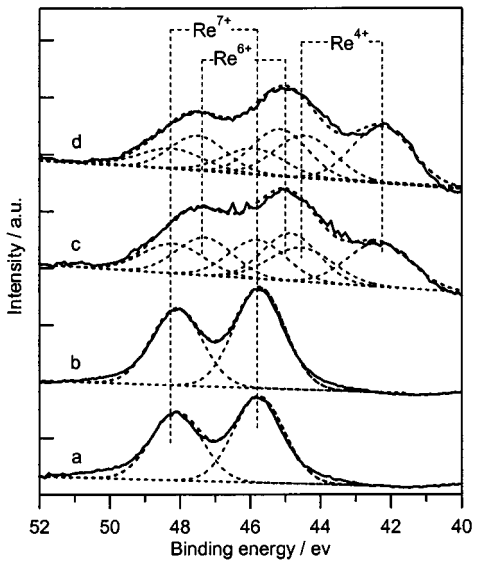

Figure 12. Re 4f XPS spectra for fresh $SbOReO_4 \cdot 2H_2O$ (a) and $Sb_4Re_2O_{13}$ (b), and $SbOReO_4 \cdot 2H_2O$ (c) and $Sb_4Re_2O_{13}$ (d) after the i-C_4H_{10} ammoxidation at 673 K for 3 h.

3.5. Characterization of the Catalysts. *3.5.1. XRD.* Figure 9 shows XRD patterns for the $SbRe_2O_6$ catalyst before and after the pretreatments with He and NH_3/He at 673 K, as well as after the i-C_4H_{10} ammoxidation reactions at 673 and 773 K for 3 h. It was found that the XRD patterns after these treatments and the i-C_4H_{10} ammoxidation were identical to that for the fresh sample. The results demonstrated that the $SbRe_2O_6$ catalyst is stable under the reaction conditions at 673−773 K. Figure 10 shows XRD patterns for $Sb_4Re_2O_{13}$ and $SbOReO_4 \cdot 2H_2O$ before and after the i-C_4H_{10} ammoxidation at 673 K. For $Sb_4Re_2O_{13}$, the XRD pattern did not change essentially after the i-C_4H_{10} ammoxidation at 673 K for 3 h, but a new weak peak appeared at 2θ angle of 27.8°. The new peak was attributable to Sb_2O_3. A drastic change in crystal structure was

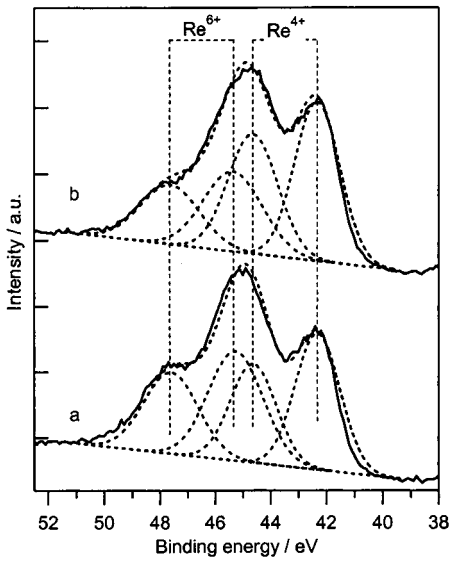

Figure 13. Re 4f XPS spectra for copr.$SbRe_2O_x$ after pretreatment under He at 673 K for 1 h (a) and after the i-C_4H_{10} ammoxidation at 673 K for 3 h (b).

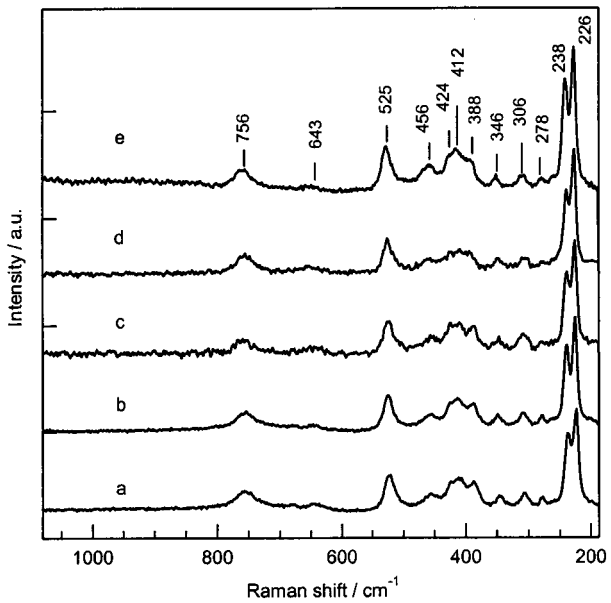

Figure 14. In situ confocal laser Raman microscopic spectra for fresh $SbRe_2O_6$ (a) and $SbRe_2O_6$ after the pretreatments under He (b) and NH_3/He (c) at 673 K for 1 h, and after the i-C_4H_{10} ammoxidation at 673 K (d) and 773 K (e) for 3 h.

observed with $SbOReO_4 \cdot 2H_2O$ after the i-C_4H_{10} ammoxidation at 673 K as shown by the XRD patterns of Figure 10a,c). The XRD pattern of Figure 10c was similar to that for $Sb_4Re_2O_{13}$ after the ammoxidation (Figure 10d).

3.5.2. XPS Spectra. Figure 11 shows Re 4f XPS spectra for the $SbRe_2O_6$ catalysts before and after the pretreatments with He and NH_3/He at 673 K, as well as after the i-C_4H_{10} ammoxidation at 673 and 773 K. In Figure 11a for fresh $SbRe_2O_6$, three peaks were observed at binding energies of 42.3, 44.8, and 47.7 eV. The peak at 42.3 eV is assigned to Re $4f_{7/2}$ for Re^{4+}[22]. The peak at 47.7 eV is assigned to Re $4f_{5/2}$ probably for Re^{6+} as discussed hereinafter.[22] Thus the most intense peak around 44.8 eV should be superimposed of Re $4f_{5/2}$ of Re^{4+} and Re $4f_{7/2}$ of Re^{6+}. We have deconvoluted the XPS spectra as shown in Figure 11. The Re^{4+} $4f_{5/2}$ and Re^{6+} $4f_{7/2}$ peaks were observed at 44.7 and 45.3 eV, respectively. The $SbRe_2O_6$ sample after the pretreatment under He at 673 K (Figure 11b)

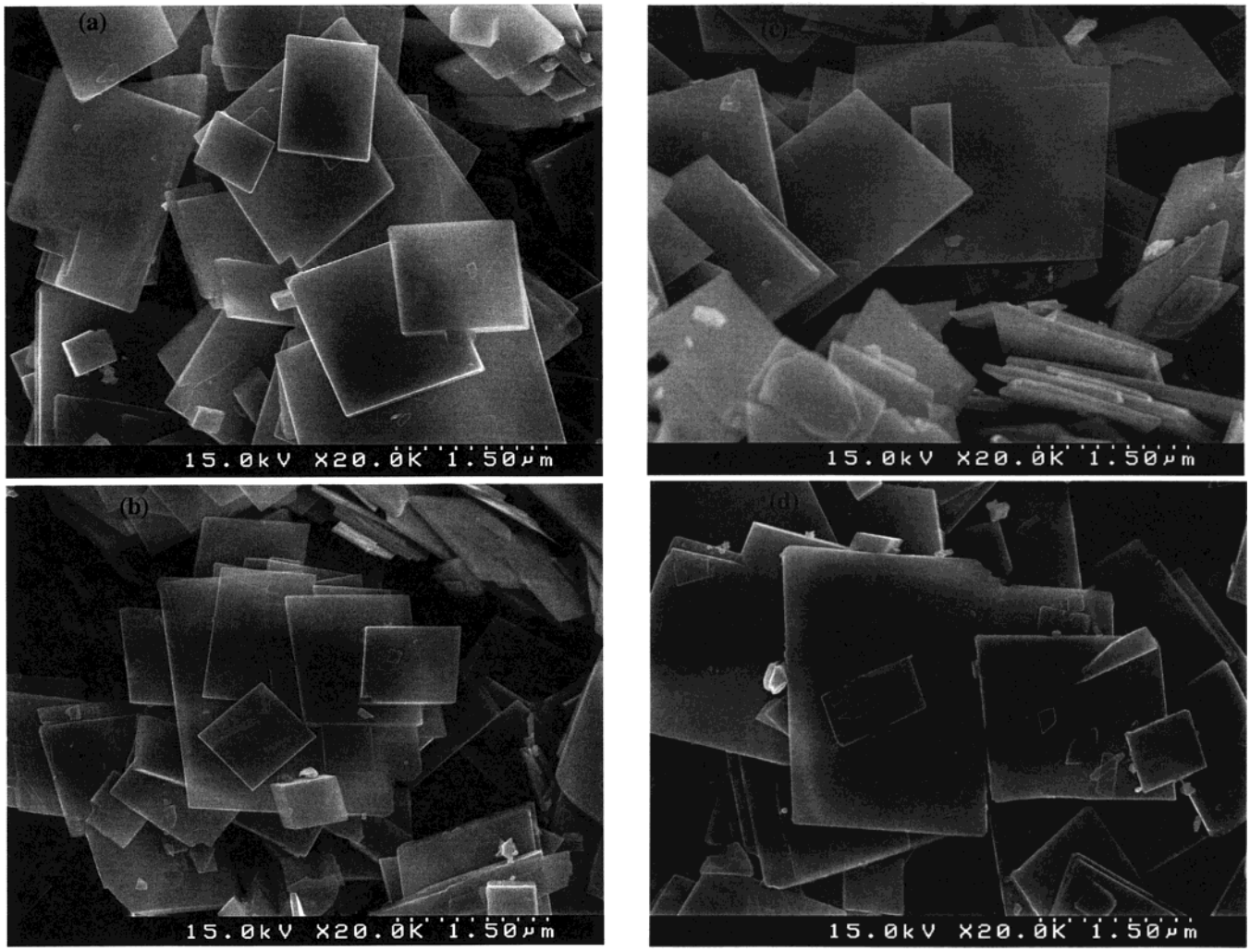

Figure 15. Scanning electron micrographs for fresh $SbRe_2O_6$ (a), and $SbRe_2O_6$ after the NH_3 pretreatment at 673 K for 1 h (b), and the *i*-C_4H_{10} ammoxidation at 673 K (c) and 773 K (d) for 3 h.

exhibited no significant difference in the XPS spectra from the fresh sample (Figure 11a). After the treatment with NH_3/He at 673 K for 1 h, the intensity of the peaks at 47.7 and 45.3 eV reduced, while the intensity of the peaks at 44.7 and 42.3 eV increased relatively (Figure 11c). The XPS spectra for the samples after the *i*-C_4H_{10} ammoxidation at 673 and 773 K for 3 h (Figure 11d,e) were similar to those for the fresh and He-treated samples (Figure 11a,b). Fresh $SbOReO_4 \cdot 2H_2O$ and $Sb_4Re_2O_{13}$ samples with Re^{7+} possessed spectra similar to each other, exhibiting two peaks centered at 45.7 and 48.1 eV (Figure 12). The peaks are attributed to the Re $4f_{7/2}$ and Re $4f_{5/2}$ levels of Re^{7+} species, respectively. After the ammoxidation reaction at 673 K for 3 h, the spectra changed drastically to show three peaks at 42.3, 44.9, and 47.4 eV. We have deconvoluted the spectra by assuming Re^{6+} and Re^{4+} species, but the fitting never reproduced the observed spectra. In consequence, the fitting was performed by assuming three different oxidation states of Re. The results are shown in Figure 12c,d. The deconvoluted peaks at 42.3 and 44.7 eV are assigned to Re $4f_{7/2}$ and Re $4f_{5/2}$ peaks for Re^{4+}, respectively, the peaks at 45.1 and 47.5 eV are assigned to Re $4f_{7/2}$ and Re $4f_{5/2}$ peaks for Re^{6+}, respectively, and the peaks at 45.8 and 48.2 eV are assigned to Re $4f_{7/2}$ and Re $4f_{5/2}$ peaks for Re^{7+}, respectively. Similar to $SbRe_2O_6$, copr.$SbRe_2O_x$ after the He pretreatment at 673 K also possessed three peaks which appeared at 47.6, 45.0, and 42.3 eV, as shown in Figure 13a. The spectrum was deconvoluted, and four peaks at 47.6, 45.2, 44.7, and 42.3 eV were observed, which are also assigned to Re $4f_{7/2}$ and Re $4f_{5/2}$ peaks for Re^{6+} and Re^{4+} species, respectively. After the *i*-C_4H_{10} ammoxidation at 673 K for 3 h, the peaks showed the same binding energies, but their intensity changed. The intensity of the peaks at 47.7 and 45.3 eV reduced, while the intensity of the peaks at 44.7 and 42.3 eV increased relatively (Figure 13b). It is to be noted that for the three Re−Sb−O compounds and copr.$SbRe_2O_x$, Sb 4d and Sb $3d_{3/2}$ binding energies around 34.5 and 539.8 eV, respectively, due to Sb^{3+} were independent of the pretreatments and the reaction.

3.5.3. LRM Spectra. The $SbRe_2O_6$ catalysts before and after the pretreatments under He and NH_3/He at 673 K, as well as after the *i*-C_4H_{10} ammoxidation at 673 and 773 K, were also investigated by in situ LRM. As shown in Figure 14, The $SbRe_2O_6$ catalysts possessed Raman features at 226 (vs) (most intense peak), 238 (s), 278 (w), 306 (w), 346 (w), 388 (m), 412 (m), 424 (m), 456 (w), 525 (m), 643 (w), and 756 (m) cm^{-1} in the range 1100−185 cm^{-1}. After the pretreatments under He and NH_3/He, and the *i*-C_4H_{10} ammoxidation, the Raman shifts essentially remained unchanged.

3.5.4. SEM Images. Figure 15 shows the SEM micrographs for the $SbRe_2O_6$ catalysts before and after the NH_3 pretreatment at 673 K for 1 h, and the *i*-C_4H_{10} ammoxidation at 673 and 773 K. Fresh $SbRe_2O_6$ was composed of crystals possessing square basal faces with 0.5−3 μm in dimension and about 100 nm thick. The basal (100) faces were smooth and possessed sharp and regular edges. After the NH_3 pretreatment and the *i*-C_4H_{10}

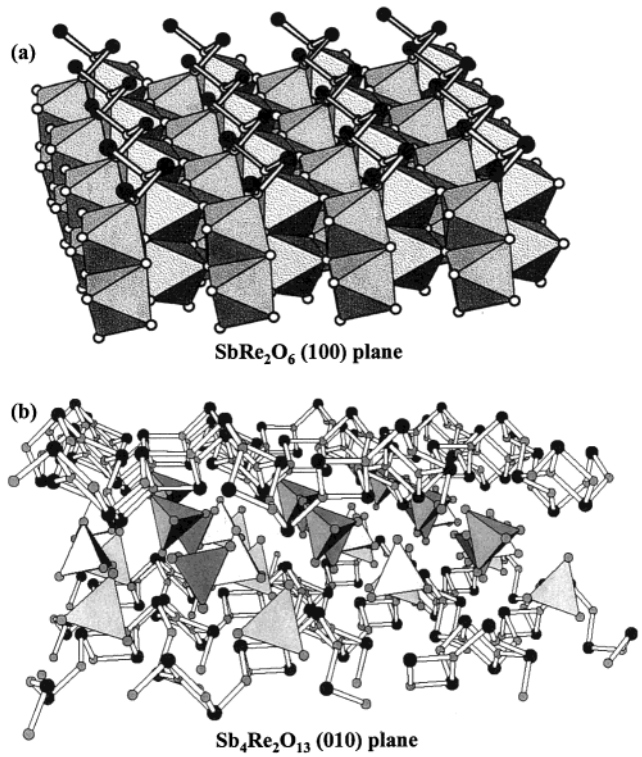

Figure 16. (a) $SbRe_2O_6$ (100) plane as a major exposed plane of $SbRe_2O_6$ crystal; Re ions are located inside oxygen octahedra and Sb ions are shown with black circles. Small white circles are O ions. (b) $Sb_4Re_2O_{13}$ (010) plane as a major exposed plane of $Sb_4Re_2O_{13}$ crystal; Re ions are located inside oxygen tetrahedra and Sb ions are shown with black circles. Small gray circles are O ions.

ammoxidation, the $SbRe_2O_6$ crystals exhibited morphology similar to that for the fresh sample.

4. Discussion

4.1. Performances and Structures of the Three Crystalline Re−Sb−O Catalysts in the *i*-C_4H_{10} Ammoxidation. It was found that among the catalysts examined in Table 1, only the crystalline $SbRe_2O_6$ efficiently catalyzed the selective ammoxidation of *i*-C_4H_{10} to MAN at 673 K, whereas the other two crystalline Re−Sb−O compounds, $SbOReO_4 \cdot 2H_2O$ and $Sb_4Re_2O_{13}$, and the other samples, including copr.$SbRe_2O_x$, mix.$Re_2O_7 \cdot Sb_2O_3$, Re_2O_7/Sb_2O_3, bulk Re oxides, and Sb oxides showed no or negligible activity for the MAN formation. The superiority of the $SbRe_2O_6$ catalyst may provide information on a key structural issue to generate the *i*-C_4H_{10} ammoxidation catalysis.

The active $SbRe_2O_6$ ($Re^{4.5+}$; Sb^{3+}) compound consists of an alternate octahedral $(Re_2O_6)^{3-}$ layer and $(SbO)^+$ layer, which are connected with each other along the (100) plane as shown in Figure 16a.[34] $SbRe_2O_6$ crystal grows preferentially along the (100) plane. This crystal structure is maintained under the catalytic ammoxidation conditions as evidenced by XRD (Figure 9), XPS (Figure 11), in-situ LRM (Figure 14), and SEM (Figure 15), which reveal neither change nor modification in the bulk and surface of $SbRe_2O_6$. Thus the $SbRe_2O_6$ crystal can work as a new promising catalyst for the *i*-C_4H_{10} ammoxidation. However, destruction of the $SbRe_2O_6$ surface takes place by a partial decomposition of $SbRe_2O_6$ to $Sb_4Re_2O_{13}$ and Re_2O_7 under O_2/He at 673 K,[5,31,32] and as a result the O_2/He-pretreated catalyst is deactivated as shown in Table 2, because $Sb_4Re_2O_{13}$ and Re_2O_7 are inactive for the MAN synthesis as shown in Table 1.

The crystalline compounds $SbOReO_4 \cdot 2H_2O$ (Re^{7+}; Sb^{3+}) and $Sb_4Re_2O_{13}$ (Re^{7+}; Sb^{3+}) are built up from tetrahedral $(ReO_4)^-$ anions and cationic $(SbO)^+$ layers.[24,33] $Sb_4Re_2O_{13}$ crystal grows preferentially along the (010) plane as shown in Figure 16b. In accordance with their formulas, the XPS spectra (Figure 12a,b for Re) reveal the oxidation states of Re and Sb to be 7+ and 3+, respectively. After the *i*-C_4H_{10} ammoxidation at 673 K, the XPS spectra for $SbOReO_4 \cdot 2H_2O$ and $Sb_4Re_2O_{13}$ dramatically changed, and were reproduced only by the sum of the $4f_{7/2}$ and $4f_{5/2}$ peaks for Re^{7+}, Re^{6+} and Re^{4+} species (Figure 12c,d). In addition, Sb_2O_3 formation was observed by XRD in Figure 10. It is evident that the reduction of Re^{7+} species in the two Re−Sb−O compounds to Re^{6+} and Re^{4+} states occurs under the ammoxidation conditions. Thus the surface layers of $SbOReO_4 \cdot 2H_2O$ and $Sb_4Re_2O_{13}$ with Re species in the 7+ oxidation state are transformed to the similar surfaces to the $SbRe_2O_6$ catalyst surfaces with Re^{6+} and Re^{4+} species after the ammoxidation at 673 K. Nevertheless, the $SbRe_2O_6$ catalyst was much more superior to the $SbOReO_4 \cdot 2H_2O$ and $Sb_4Re_2O_{13}$ catalysts. There may be two possibilities for the difference in their performances. A possible idea is to assume that $SbOReO_4 \cdot 2H_2O$ and $Sb_4Re_2O_{13}$ may be active but the inactive Sb_2O_3 produced by their decomposition covers the catalyst surfaces, resulting in no activity. To examine this possibility, pulse experiment was conducted on $Sb_4Re_2O_{13}$ at 673 K, where only a small portion of $Sb_4Re_2O_{13}$ decomposed by every pulse, but no *i*-C_4H_{10} conversion was observed. The case of $SbOReO_4 \cdot 2H_2O$ was the same. These results indicate that $Sb_4Re_2O_{13}$ and $SbOReO_4 \cdot 2H_2O$ are intrinsically inactive for the *i*-C_4H_{10} ammoxidation. Therefore, another possibility is more plausible that the difference in the catalytic performances of the three crystalline Re−Sb−O catalysts may be due to the difference in their surface structures rather than the difference in their surface Re oxidation states. This can also account for the incapability of the copr.$SbRe_2O_x$ catalyst for the *i*-C_4H_{10} ammoxidation to MAN, which also possesses the Re^{6+} and Re^{4+} species similar to those in $SbRe_2O_6$ (Figure 13). This is entirely different from the finding in the selective oxidation of *i*-C_4H_{10} and *i*-C_4H_8 to MAL that the activities of the three crystalline Re−Sb−O compounds are ascribed to a cooperation between Re_2O_7 and $Sb_4Re_2O_{13}$, both being formed on these Re−Sb−O compounds under the oxidizing conditions.[5,31,32]

In contrast to these *i*-C_4H_{10} ammoxidation results, for the *i*-C_4H_8 ammoxidation to MAN, all the Re-containing samples listed in Table 1 were more or less active at 673 K, though the $SbRe_2O_6$ catalyst is much more superior to other samples in both activity and MAN selectivity.[37] It is suggested from the comparison with the *i*-C_4H_8 ammoxidation that the different performances of the Re−Sb−O catalysts in the *i*-C_4H_{10} ammoxidation lie in the difference in their activity for the C−H bond activation of *i*-C_4H_{10} to form *i*-C_4H_8. The structural characteristic of the $SbRe_2O_6$ catalyst mentioned above (Figure 16) may meet the requirement for the *i*-C_4H_{10} activation to form *i*-C_4H_8 and the *i*-C_4H_8 to allyl species at 673 K. Next, we focus the discussion on this promising $SbRe_2O_6$ catalyst.

4.2. Role of NH_3 in the *i*-C_4H_{10} Ammoxidation on $SbRe_2O_6$. It is to be noted that in the absence of NH_3 $SbRe_2O_6$ was inactive for both selective and total oxidation of *i*-C_4H_{10}, whereas it exhibited good performance for the *i*-C_4H_{10} ammoxidation in the steady-state flow of a mixture of *i*-C_4H_{10}/NH_3/O_2/He at 673 K (Table 1, Figure 7). This is in contrast to the case of *i*-C_4H_8 ammoxidation, in which the *i*-C_4H_8 ammoxidation to MAN on $SbRe_2O_6$ proceeded in the presence of NH_3, and the selective oxidation of *i*-C_4H_8 to MAL also proceeded

efficiently at 673 K in the absence of NH_3.[37] Thus it is evident that NH_3 promotes the C−H bond breaking in i-C_4H_{10} (dehydrogenation). The pulse experiments in Figure 7 demonstrate that adsorbed NH_3 species are incorporated to the ammoxidation of i-C_4H_{10} to form MAN. It is also evident that NH_3 not only behaves as a reactant in the i-C_4H_{10} ammoxidation but also plays a crucial role in enhancing and/or generating the activity of $SbRe_2O_6$ for the dehydrogenation of i-C_4H_{10} to i-C_4H_8.

The adsorption of NH_3 on the $SbRe_2O_6$ catalyst at room-temperature developed the O−H and N−H peaks centered at 3736 and 3331 cm^{-1}, respectively, as shown in Figure 8. The appearance of the OH peak provides an evidence that NH_3 dissociatively adsorbs on the catalyst. The intensity of the two peaks increased significantly by exposure to NH_3 at 673 K, followed by cooling to room temperature, indicating that the NH_3 dissociation is favored at high temperature. The adsorbed species may be formed through the reaction of NH_3 with the lattice oxygen (O^*) of $SbRe_2O_6$. In combination with the XPS result that the higher oxidation state Re^{6+} species was reduced after the pretreatment with NH_3 at 673 K (Figure 11, curve c), it is suggested that NH_3 reacts with the lattice oxygen atoms on Re^{6+} to form NH_x ($x = 1$ or 2) species and OH groups. The subsequent introduction of the i-C_4H_{10}/O_2 mixture at 673 K led to the disappearance of the N−H band at 3331 cm^{-1}, while the O−H band at 3736 cm^{-1} remained almost unchanged (Figure 8, curve d). Hence, the NH_x species are active species for the i-C_4H_{10} ammoxidation. Due to the low transmittance of the black sample, unfortunately the absorption bands of the NH_x species in the bending vibration region cannot be observed, so it is difficult to discriminate NH or NH_2 for the NH_x species. A similar conclusion was claimed by Sokolovskii et al. in propane ammoxidation on Ga−Sb oxides, where NH_2 amide species detected by IR were suggested to be responsible for the reaction.[3] Andersson and co-workers also suggested that amide-like species participated in the propane ammoxidation on Sb−V−O catalysts,[12] whereas Centi et al. reported that NH_3 undissociatively adsorbed on the Sb−V−O catalysts.[38,39] The promoting effect of NH_3 on the selective ammoxidation catalyses is more remarkable on the $SbRe_2O_6$ catalyst than on others. The other mixed-oxides are more or less active for the alkane oxidation in the absence of NH_3, whereas the $SbRe_2O_6$ catalyst was completely inactive in the absence of NH_3. To our knowledge, $SbRe_2O_6$ is the first oxide among oxide catalytic systems that NH_3 transforms an inactive catalyst to an active catalyst for the light alkane activation.

In addition, as discussed above, the crystal structure of $SbRe_2O_6$ does not change after the i-C_4H_{10} ammoxidation at 673 and 773 K, whereas the $SbRe_2O_6$ surface layers decompose to Re_2O_7 and $Sb_4Re_2O_{13}$ at 673 K in the absence of NH_3. It demonstrates that NH_3 also plays an important role in maintaining the crystal structure of $SbRe_2O_6$ under the catalytic reaction conditions.

4.3. Catalytic Properties of $SbRe_2O_6$ and Mechanism for the Ammoxidation. The i-C_4H_{10} conversion increased with an increase of reaction temperature, passed through a maximum at 673 K, and dropped to a low level above 750 K, as shown in Figure 2. No change in the bulk and at the surface of $SbRe_2O_6$ occurred after the ammoxidation over the whole temperature range as characterized by XRD (Figure 9), XPS (Figure 11), LRM (Figure 14), and SEM (Figure 15). So the sharp decline in the activity above 673 K is not relevant to any structural change of the catalyst. There may be two possible explanations. Higher temperatures may facilitate the combustion of adsorbed NH_3 species with oxygen on the $SbRe_2O_6$ surface, resulting in the low activity of the ammoxidation. But this possibility is excluded by the NH_3 and O_2 conversions measured during the ammoxidation reaction. It is also excluded by the result of the i-C_4H_8 ammoxidation that the activity at 773 K is much higher than that at 673 K. Therefore, it is more plausible that the low activity above 673 K is due to the decrease in the amount of i-C_4H_{10} adsorbed on the catalyst. The temperature dependence profile in Figure 2 may reflect a change in the rate-determining step of the i-C_4H_{10} ammoxidation on $SbRe_2O_6$. Below 673 K, the reaction rate is limited by the dehydrogenation rate of a C−H bond in i-C_4H_{10}, and above 673 K the adsorption of i-C_4H_{10} on the catalyst surface determines the reaction rate.

It is to be noted that the selectivity to MAN remained unchanged at the higher temperatures, that is to say, higher temperatures never increased the formation of byproducts such as acetonitrile and CO_2 as shown in Figure 2. The MAN selectivity did not change significantly when the i-C_4H_{10} conversion increased so much by decreasing GHSV (Figure 1). This is a unique catalytic property of the new $SbRe_2O_6$ catalyst.

The i-C_4H_8 formation rate was of first order with respect to the i-C_4H_{10} partial pressure, while it followed partial order dependencies on the pressures of O_2 and NH_3 (between 5 and 15 kPa) (eq 4). From these results we can assume that the C−H cleavage in C_4H_{10} to form i-C_4H_8 is the rate-determining step in the i-C_4H_{10} ammoxidation at 673 K. The MAN formation rate follows a partial order rate dependence with respect to the i-C_4H_{10} pressure, which indicates that MAN is not produced directly from i-C_4H_{10} but from an intermediate species, probably i-C_4H_7 (methallyl) in the successive steps i-$C_4H_{10} \rightarrow i$-$C_4H_8 \rightarrow i$-$C_4H_7 \rightarrow$ MAN.[6−8] Thanks to the competitive adsorption of i-C_4H_8 and NH_3 on $SbRe_2O_6$,[37] the concentration of the i-C_4H_8 intermediate in the i-C_4H_{10} ammoxidation should be much lower than that of reactant NH_3. This explains why the high i-C_4H_8 selectivity (∼40%) is obtained in the i-C_4H_{10} ammoxidation, although the i-C_4H_8 ammoxidation proceeds faster by a factor of about 5 than the i-C_4H_{10} ammoxidation. Adsorption of i-C_4H_{10} is weaker than that of NH_3, so the rates of the MAN and i-C_4H_8 formations decrease through maxima with increasing NH_3 pressure (Figure 5). Similar rate dependencies were observed on V−Sb oxides in propane ammoxidation.[12,38]

It is generally accepted that selective oxidation and ammoxidation of hydrocarbons on mixed-metal oxides occur by a Mars-van Krevelen redox.[11,40−42] The important contribution of lattice oxygen to the ammoxidation of i-C_4H_{10} to MAN on $SbRe_2O_6$ at 673 K can be seen in Figure 6. Because the lattice oxygen atoms of $SbRe_2O_6$ are consumed by reaction with NH_3, which is indeed evidenced by the formation of N_2 and H_2O upon pulsing NH_3, the MAN and i-C_4H_8 yields at the first pulse of the i-C_4H_{10}/NH_3/He mixture on the steady-state $SbRe_2O_6$ catalyst were as low as 10% of the steady-state values as shown in Figure 6. However, the consumed lattice oxygen atoms were rapidly replenished by pulsing the reaction mixture of i-$C_4H_8/NH_3/O_2$/He, and the steady-state activity was recovered (Figure 6). The XPS spectra in Figure 11 also reveal a partial reduction of Re^{6+} species to Re^{4+} species by pretreatment of $SbRe_2O_6$ with NH_3/He at 673 K and the recovery of the original species under the ammoxidation reaction condition. The amount of lattice oxygen atoms consumed in the reactions with NH_3 and with i-C_4H_{10} was estimated to be approximately 5.1×10^{17}, which corresponds to about 11% of the surface lattice oxygen atoms (ca. 4.5×10^{18}) of the catalyst (0.45 g), assuming the surface oxygen density to be roughly 10^{19} atoms m^{-2}.[43] The replenishment of the surface oxygen atoms by bulk oxygen atoms at 673 K is slow, while the consumed surface oxygen atoms are replenished

rapidly by gas-phase oxygen. The gas-phase oxygen does not promote the i-C_4H_{10} combustion to CO_2 as shown in Figure 4. As suggested by XPS, the active oxygen atoms are bound to the Re^{6+} species that are connected with the $Sb^{3+}-O-Sb^{3+}$ chains at the $SbRe_2O_6$ surface.

5. Conclusions

(1) Among the three crystalline Re−Sb−O compounds, $SbRe_2O_6$, $SbOReO_4 \cdot 2H_2O$, and $Sb_4Re_2O_{13}$, only $SbRe_2O_6$ catalyzed the selective ammoxidation of i-C_4H_{10} to MAN and also the selective dehydrogenation of i-C_4H_{10} to i-C_4H_8 at 673−773 K with a high selectivity.

(2) No structural change in the bulk and at the surface of $SbRe_2O_6$ after the i-C_4H_{10} ammoxidation was observed by XRD, XPS, LRM, and SEM. The good performance of $SbRe_2O_6$ may be relevant to its specific crystal structure with alternate octahedral $(Re_2O_6)^{3-}$ and $(SbO)^+$ layers connected with each other through Re−O−Sb bonds.

(3) The presence of NH_3 in the i-C_4H_{10} ammoxidation not only behaved as reactant but also played a crucial role in maintaining the crystal structure of $SbRe_2O_6$ and further generated the activity of the catalyst for breaking the C−H bond in i-C_4H_{10}. In the absence of NH_3 neither oxidation nor dehydrogenation of i-C_4H_{10} proceeded.

(4) NH_3 reacted with the lattice oxygen of $SbRe_2O_6$ surface to form an NH_x species and oxygen vacancies, which are responsible for the ammoxidation activity of the $SbRe_2O_6$ catalyst.

(5) The i-C_4H_{10} ammoxidation on the $SbRe_2O_6$ catalyst took place by a redox mechanism involving the surface oxygen atoms on Re^{6+}.

(6) The activation of the C−H bond in i-C_4H_{10} to form i-C_4H_8 was the rate-determining step in the i-C_4H_{10} ammoxidation, followed by further dehydrogenation of i-C_4H_8 to i-C_4H_7 (methallyl) and subsequent insertion of NH_x species to the i-C_4H_7 intermediate to yield MAN.

(7) The selectivity to MAN and i-C_4H_8 did not decrease by increasing reaction temperature and decreasing GHSV, where undesirable increase in the formation of byproducts such as CO_2 and acetonitrile was not observed, which marks the crystalline $SbRe_2O_6$ as a promising catalyst for alkane ammoxidation.

Acknowledgment. This work has been supported by Core Research for Evolutional Science and Technology (CREST) of Japan Science and Technology Corporation (JST). The SEM measurements were conducted in the Electron Microbeam Analysis Facility of the Mineralogical Institute, The University of Tokyo.

References and Notes

(1) Grasselli, R. K. *Catal. Today* **1999**, *49*, 141.
(2) Albonetti, S.; Cavani, F.; Trifiro, F. *Catal. Rev.−Sci. Eng*. **1996**, *38*, 413.
(3) Sokolovskii, V. D.; Davydov, A. A.; Ovsitser, O. Yu. *Catal. Rev.−Sci. Eng*. **1995**, *37*, 425.
(4) Nilsson, J.; Land-Canovas, A. R.; Hansen, S.; Andersson, A. *J. Catal*. **1999**, *186*, 442.
(5) Liu, H.; Gaigneaux, E. M.; Imoto, H.; Shido, T.; Iwasawa, Y. *Appl. Catal. A: General* **2000**, *202*, 251.
(6) Inoue, T.; Oyama, S. T.; Imoto, H.; Asakura, K.; Iwasawa, Y. *Appl. Catal. A: General* **2000**, *191*, 131.
(7) Inoue, T.; Asakura, K.; Iwasawa, Y. *J. Catal*. **1997**, *171*, 184.
(8) Inoue, T.; Asakura, K.; Iwasawa, Y. *J. Catal*. **1997**, *171*, 457.
(9) Cassidy, T. J.; Pollastri, M.; Trifiro, F. *J. Catal*. **1997,** *172*, 55.
(10) Ushikubo, T.; Oshima, K.; Kayou, A.; Vaarkamp, M.; Hatano, M. *J. Catal*. **1997**, *169*, 394.
(11) Zanthoff, H.-W.; Buchhloz, S. A. *Catal. Lett*. **1997**, *49*, 213.
(12) . Nilsson, R.; Lindblad, T.; Anderson, A. *J. Catal*. **1994**, *148*, 501.
(13) Ruth, K.; Kieffer, R.; Burch, R. *J. Catal*. **1998**, *175*, 16.
(14) Asakura, K.; Nakatani, K.; Kubota, T.; Iwasawa, Y. *J. Catal*. **2000**, *194*, 309.
(15) Wachs, I. E.; Deo, G.; Andreini, A.; Vuurman, M. A.; de Boer, M. *J. Catal*. **1996**, *190*, 322.
(16) Chen, K.; Bell, A. T.; Iglesia, E. *J. Phys. Chem. B* **2000**, *104*, 1292.
(17) Moro-oka, Y.; Ueda, W. *Adv. Catal*. **1994**, *40*, 233.
(18) Kung, H. H. *Adv. Catal*. **1994**, *40*, 1.
(19) Kim, D. S.; Wachs, I. E. *J. Catal*. **1993**, *141*, 419.
(20) Wang, C.-B.; Cau, Y.; Wachs, I. E. *Langmuir* **1999**, *15*, 1223.
(21) Yuan, Y.; Shido, T.; Iwasawa, Y. *Chem. Commun*. **2000**, 1421.
(22) Yuan, Y.; Liu, H.; Imoto, H.; Shido, T.; Iwasawa, Y. *J. Catal*. **2000**, *195*, 51.
(23) Yuan, Y.; Liu, H.; Imoto, H.; Shido, T.; Iwasawa, Y. *Chem. Lett*. **2000**, 674.
(24) Harrison, W. T. A.; McManus, A. V. P.; Kaminsky, A. P.; Cheetham, A. K. *Chem. Mater*. **1993**, *5*, 1631.
(25) Pillep, B.; Behrens, P.; Schubert, U.-A.; Spengler, J.; Knözinger, H. *J. Phys. Chem. B* **1999**, *103*, 9595.
(26) Allen, M. D.; Poulston, S.; Bithell, E. G.; Goringe, M. J.; Bowker, M. *J. Catal*. **1996**, *163*, 204.
(27) Poulston, S.; Price, N. J.; Weeks, C.; Allen, M. D.; Parlett, P.; Steinberg, M.; Bowker, M. *J. Catal*. **1998**, *178*, 658.
(28) Delmon, B.; Froment, G. F. *Catal. Rev.−Sci. Eng*. **1996**, *38*, 69.
(29) Centi, G.; Trifiro, F. *Catal. Rev.−Sci. Eng*. **1986**, *28*, 165.
(30) Berry, F. J. *Adv. Catal*. **1981**, *30*, 97.
(31) Liu, H.; Gaigneaux, E. M.; Imoto, H.; Shido, T.; Iwasawa, Y. *J. Phys. Chem. B* **2000**, *104*, 2033.
(32) Gaigneaux, E. M.; Liu, H.; Imoto, H.; Shido, T.; Iwasawa, Y. *Topics Catal*. **2000**, *11−12*, 185.
(33) Watanabe, H.; Imoto, H. *Inorg. Chem*. **1997**, *36*, 4610.
(34) Watanabe, H.; Imoto, H.; Tanaka, H. *J. Solid State Chem*. **1998**, *138*, 245.
(35) Liu, H.; Shido, T.; Iwasawa, Y. *Shokubai (Catalysts and Catalysis)* **2000**, *42*, 70.
(36) Liu, H.; Shido, T.; Iwasawa, Y. *Chem. Commun*. **2000**, 1881.
(37) Liu, H.; Imoto, H.; Shido, T.; Iwasawa, Y. *J. Catal*. **2001**, *200*, 69.
(38) Centi, G.; Perathoner, S. *Catal. Rev.−Sci. Eng*. **1998**, *40*, 175.
(39) Centi, G.; Marchi, F.; Perathoner, S. *Appl. Catal. A* **1997**, *149*, 225.
(40) Mars, P.; van Krevelen, D. W. *Chem. Eng. Sci*. **1954**, *3*, 41.
(41) Knietzni, K. F.; Zanthoff, H. W.; Maier, W. F. *J. Catal*. **1999**, *188*, 154.
(42) Haber, J.; Turek, W. *J. Catal*. **2000**, *190*, 320.
(43) Winter, E. R. S. *J. Chem. Soc. A* **1968**, 2889.